Renewable Energy 114 (2017) 1051–1061

Contents lists available at ScienceDirect

Renewable Energy

journal homepage: www.elsevier.com/locate/renene

A hybrid prognostic methodology for tidal turbine gearboxes

Faris Elasha [a, *], David Mba [b], Michael Togneri [c], Ian Masters [c], Joao Amaral Teixeira [d]

[a] Faculty of Engineering, Environment and Computing, Coventry University, UK
[b] London South Bank University, London, UK
[c] Swansea University, Swansea, UK
[d] Cranfield University, Bedfordshire, UK

ARTICLE INFO

Article history:
Received 28 December 2015
Received in revised form
14 December 2016
Accepted 23 July 2017
Available online 24 July 2017

Keywords:
Tidal turbines
Prognosis
Gearbox
Life prediction
Diagnosis
Health management

ABSTRACT

Tidal energy is one of promising solutions for reducing greenhouse gas emissions and it is estimated that 100 TWh of electricity could be produced every year from suitable sites around the world. Although premature gearbox failures have plagued the wind turbine industry, and considerable research efforts continue to address this challenge, tidal turbine gearboxes are expected to experience higher mechanical failure rates given they will experience higher torque and thrust forces. In order to minimize the maintenance cost and prevent unexpected failures there exists a fundamental need for prognostic tools that can reliably estimate the current health and predict the future condition of the gearbox.

This paper presents a life assessment methodology for tidal turbine gearboxes which was developed with synthetic data generated using a blade element momentum theory (BEMT) model. The latter has been used extensively for performance and load modelling of tidal turbines. The prognostic model developed was validated using experimental data.

1. Introduction

Power generated from Renewable energy resources in the UK in 2015 increased by 29% compared to 2014, and accounted for 25% of total UK electricity generation. Wave and tidal stream energy has the potential to meet up to 20% of the UK's current electricity demand, representing a 30-to-50 GW (GW) installed capacity. Between 200 and 300 MW (MWs) of generation capacity may be able to be deployed by 2020, and at the higher end of the range, up to 27GWs by 2050 [1,2,3].

Operation and maintenance (O&M) decisions for tidal turbines contributes significantly to the cost of tidal energy production [4]. These decisions generally depend on many factors such as machine health, repair costs, weather conditions, etc. Premature failures in gearboxes result in a significant cost increase due to unplanned maintenance and long downtime. Such gearbox failures have plagued the wind turbine industry for decades despite reasonable adherence to design practices [5]. The tidal turbine gearbox will experience higher torque, thrust and transient events [6].

Recent wind industry experience has triggered the use of essentially three main approaches for dealing with gearbox reliability; root cause analysis, improving system design and condition monitoring [7,8]. The Condition Monitoring (CM) systems of wind turbine gearboxes are commonly applied to detect damage in advance of the failure of the equipment. Efficient condition monitoring must be sensitive enough to detect potential failure events in order to provide adequate time for an operator to plan maintenance inspections and repairs [9–11]. Oil and vibration analysis have been used extensively for condition monitoring of wind turbine gearboxes [12–14]. These provide identification of changes in predetermined condition indicators (CI), and ideally should be capable of quantifying damage severity in order to estimate remaining useful life (RUL) using failure prediction models. Oil debris monitoring is more beneficial for fault identification as the majority of faults in wind turbine gearboxes are due to bearing spall and gear pitting [13]. These types of faults release metallic wear debris particles and the size and number of these particles increases with time until failure is reached. Recently a combination of oil and vibration analysis has been applied in order to efficiently predict the remaining life of bearings. This technique utilizes modern computational algorithms such as neural networks [15,16], fuzzy logics [17] and a Bayesian network [18] to predict the failure. However, varying loads and speed fluctuations provide a challenge to the application of many of these algorithms [19,20]. The

* Corresponding author.
E-mail address: faris.elasha@coventry.ac.uk (F. Elasha).

http://dx.doi.org/10.1016/j.renene.2017.07.093

availability of tidal turbines significantly affects their economic viability and a key aspect of tidal turbine availability is the need for efficient planning of maintenance resources. Condition Monitoring Systems (CMS) offer a solution to maintenance management and increased reliability [5,21–23] as demonstrated in the wind turbine industry. Such systems continuously monitor turbine components and provide an optimum maintenance schedule.

Failures in gearboxes are essentially related to the uncertainty associated with loading condition during the design phase. In addition transient loading events contribute detrimentally to fatigue life. These transient load events are caused by large variations in load condition, grid loss or resonant vibration. The former is of particular concern as the operational load variation on tidal blades has been seen to change by 100% within a few seconds, as depicted in Fig. 1. In this instance the normalised torque increased from just over 0.1 to 0.9 within 10 s. These large variations in load have a determinant effect on drivetrain mechanical integrity, and as such the continuous monitoring of the tidal loading condition can provide an effective tool for health assessment [24].

Generally, prognostic approaches can be categorized into three forms: data-driven, physics-based and fusion prognostics (hybrid) approaches. The majority of current research into gearbox prognosis uses the data-driven methodology which is based on vibration and oil analysis [9,13,26] technologies. Typically, the data is collected during operation and then statistically treated to estimate the residual life (RUL). However, for most of the developed prediction models the time between the residual life (RUL) prediction and actual failure is relatively short [27] which ultimately leads to higher maintenance costs. Physics-based models have been applied for prediction of life based on crack propagation theory; such models require significant information and are difficult to develop so they have not become established in industry [28]. Hybrid approaches combine both data-driven and physics-based information to take the advantage of the strengths of each approach while overcoming their limitations [29].

This paper introduces a hybrid prognostic approach for predicting the remaining life centred on a methodology that combines data-driven and physics-based models. The aim of this paper is to propose this new methodology as a practical tool for gearbox prognosis. In order to predict the life accurately realistic data is required, therefore data based on a hydrodynamic model has been generated for demonstrating and validating the presented prognostic model; details of the hydrodynamic model is presented in section 3".

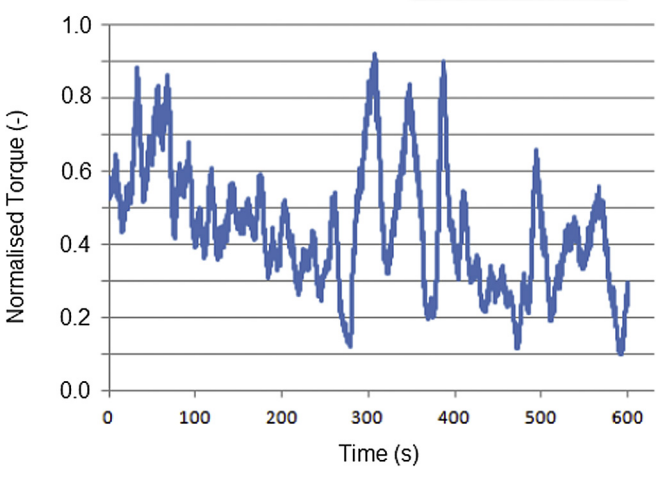

Fig. 1. Example of load variation on tidal blades based on flow prediction for Ramsey Sound site in the UK [25].

This research presents a novel approach for gear prognosis which can be used for both wind and tidal turbines. The main contributions of this work includes residual gear life estimation for tidal gearboxes based on realistic load and speed conditions, which was generated for one of UK sites earmarked for tidal power. In addition, the paper introduces a new method to generate realistic flow data based on a combination of ADCP, SEM, and BEMT.

2. Prognostic concept

Gearbox life is limited by the ability of the gear teeth to transmit power for the required number of cycles without failure. The most common gear failure modes are pitting, spalling and bending fatigue. Therefore, significant efforts have been made to minimize these failures at the design phase by considering different design characteristics. International standards for gear design [30,31] consider the life of gears for both bending and contact fatigue. The latter leads to the formation of pits which occur if the limits of the surface durability of the meshing flanks are exceeded, resulting in particles breaking out of the flanks leading to pit formation. The extent to which such pits can be tolerated (in size and number) varies within wide limits, depending mainly on the field of application. In some fields, extensive pitting can be accepted; in other fields, any appreciable pitting is to be avoided. In bending fatigue, if the load exceeds the fatigue limit, cracks are formed. The first of these often appears in the fillets where the compressive stress is generated; i.e. in the "compression fillets" which are those of the non-working flanks. Tooth breakage usually ends the service life of a transmission system. In this study, the gear failure initiation is considered as the point of end of life.

The gear design process considers numerous influences that can be generalized into material factors, geometric factors, lubrication and general influence factors. These factors were introduced to take account of the influence of many characteristics of gears such as the elasticity of the material, the helix angle of the teeth and the number of cycles in the design life. These factors were categorized into three: general influence factors (K), pitting resistance factors (Z) and bending resistance factors (Y). The general influence factors are used in both pitting and tooth bending resistance calculations and includes the application factor K_A, which accounts for the effect of variable load, the dynamic factor K_v, which makes allowance for the effects of gear tooth quality level and modifications relating to speed and load. Moreover, other load factors ($\mathbf{K_{H\beta}}$ and $\mathbf{K_{H\alpha}}$) are applied to take account of the influence of load distribution in both normal and transverse directions [30]. The pitting resistance factors include geometry factors which account for the influence of geometry characteristics to contact fatigue such as zone factor$\mathbf{Z_H}$, helix angle factor $\mathbf{Z_\beta}$ etc. In addition, pitting fatigue resistance factors account for the effect of material and oil film. An estimation methodology of pitting resistance factors is detailed in the relevant ISO standard (ISO 6336.2) [32]. The numerous bending fatigue resistance factors determine the effect of geometry and surface condition on gear root bending fatigue [33]. These influencing factors on gears life are considered in the prognostic methodology presented in this paper.

The prognostic model presented aims to evaluate the remaining life of tidal turbine gearboxes. This model is focused on predicting the residual time before failure initiation. Failure initiation is characterised by the presence of the first pit on gear flank. The size of this pit varies depending on gear modules, the gears module is the unit of size that indicates how big or small a gear is. It is the ratio of the reference diameter of the gear divided by the number of teeth, for gears with 2–5 module, the pit size that characterises a fault initiation is 0.4 mm in diameter [33]. For gears

with modules above 5 the pit size is for fault initiation is 0.8 mm in diameter [34].

A schematic representation of the proposed prognostic model is shown in Fig. 2. The model consists of four stages; the first stage consists of processing measured data (rotor speed and torque) that is employed to estimate the drive train load spectra. The second stage includes gearbox design model which estimate gear geometry and fatigue resistance factors. The third stage brings together the load spectra, gear geometry and fatigue resistance factors into a life prediction model. At this stage a series of calculations are performed to estimate the gear damage index for pitting and bending failures, the damage index represents the fraction of life consumed by exposure to the cycles at the different stress levels. In general, when the damage fraction reaches 1, failure occurs. The last stage of the model involves predicting the remaining life is predicted based on the accumulated damage index and average damage index per tidal cycle, the later continuously updated through out turbine operation.

To achieve life prediction model of tidal turbines understanding of gearbox design is essential. The main function of the tidal turbine gearboxes is to transmit the power from the low speed high torque rotor to the generator operating at high speed and low torque. Typically epicyclic gear modules are employed due to their high transmission ratio, high torque to weight ratio and high efficiency [35]. Tidal turbine gearboxes configurations are similar to those employed in wind turbines as they share similar design features such as the combined use of epicyclic and parallel gear configurations, see Fig. 3. The gearbox configuration employed for this investigation consist of two planetary stages and one parallel stage, see Fig. 3. The details of the gearbox design can be seen in Table 1. This gearbox type has been extensively studied to investigate premature wind turbine gearbox failures [5,8,36–39], as such its application to the developed prognostic model provided a source of validation.

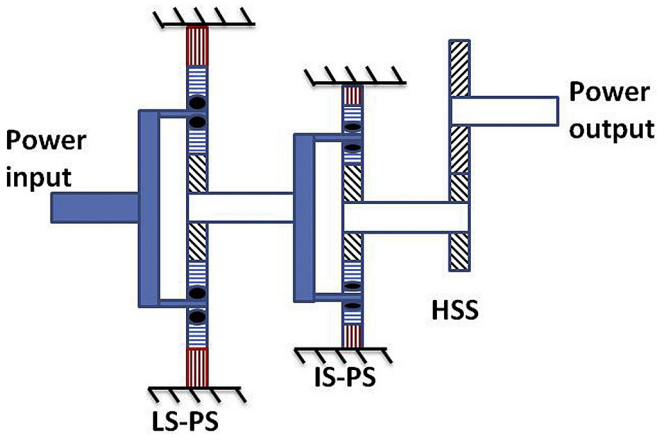

Fig. 3. Gearbox configuration (LS-PS: Low Speed Plentary stage, IS-PS Intermediated Stage Plentary Stage, HSS: High Speed Stage) [34].

2.1. Cycle counting

In the majority of applications gearboxes typically operate at rated torque throughout their life and as such the predicted gear fatigue strength is modified by 'life factors' obtained from the material characteristics. However for gearboxes subject to loads of differing amplitude stress cycles counting is required. Many traditional techniques have been suggested for stress cycles counting such as rainflow and rang-pair methods. However for tidal gearboxes the number of stress cycles does not only depend on the variable loading condition but also on the gear rotational speed, therefore the use of traditional cycle counting methods are inappropriate. To overcome this limitation the authors used the number of cycles at a particular stress level, estimated based on time spent at each load and speed, see equation (1).

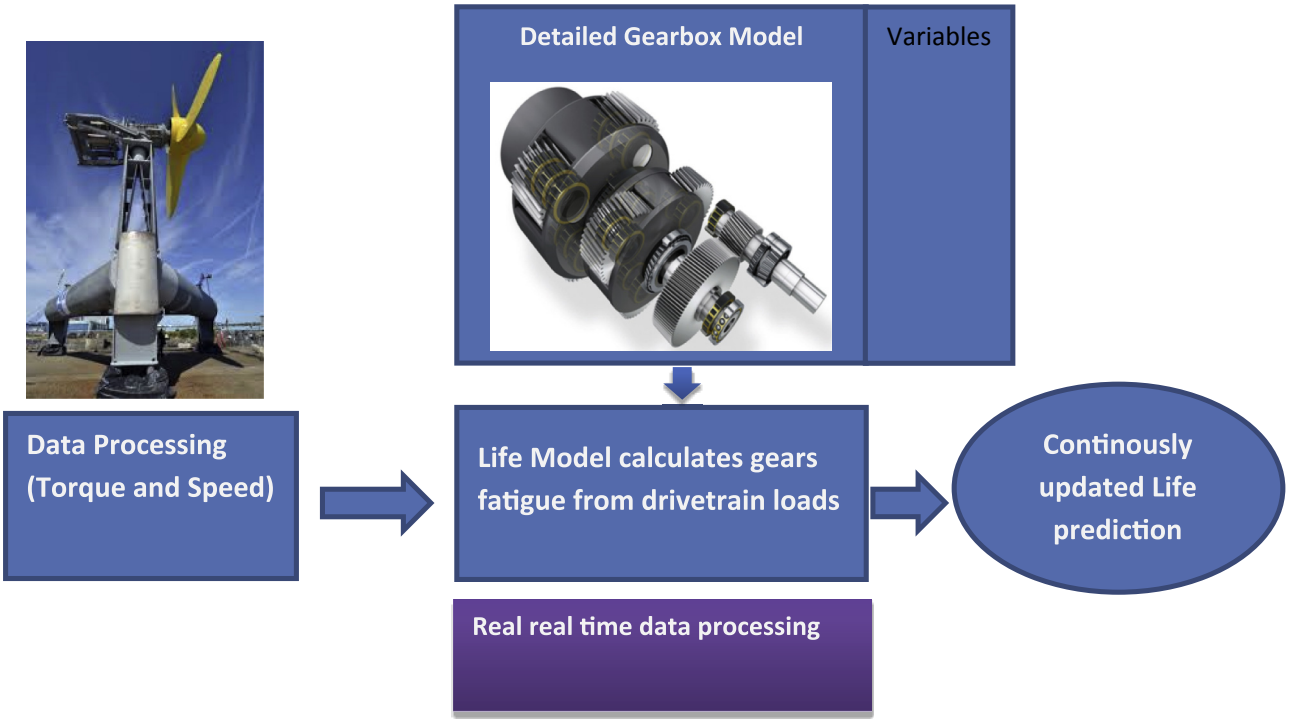

Fig. 2. Gearbox prognostic model.

Table 1
Gearbox design features.

Gear	Sun	Planet (×4)	Internal Gear
First Stage			
Number of teeth	27	47	121
Module (mm)	8		
Helix angle (°)	0		
Facewidth (mm)	90		
Centre distance (mm)	296		
Second Stage			
No teeth	25	23	75
Module (mm)	9		
Helix angle (°)	0		
Facewidth (mm)	98.5		
Centre distance (mm)	230		
Third stage			
Gear	Pinion	Wheel	
No of teeth	18	69	
Module (mm)	4		
Helix angle (°)	0		
Facewidth (mm)	54.945		
Centre distance (mm)	172		

$$N_t = \frac{\omega_t}{60} \times \frac{1}{F_{sample}} \tag{1}$$

where N_t is the number of cycles for one tooth of each gear, ω_t (rpm) is the rotating speed of the gear during the corresponding load, F_{sample} is the fraction of time corresponding to the load under consideration.

Equation (1) shows the number of cycles N_t is calculated for each data sample, so the number cycle is calculated for each load point, which generate a very dense load spectrum (load-cycle spectrum). Therefore data reduction is important to avoid computationally expensive data processing. Data reduction was achieved by accumulation load cycles into a load spectrum with a larger bin size. The first step in constructing this spectrum is to divide the entire load range of values into a series of intervals and then count how many cycles at the same load fall into each interval.

Ideally the prognostic model should use data from operational measurements of torque and speed. However, for the purposes of this investigation, data from the numerical simulation described in section 3 was employed. With the torque data the corresponding load on gears were estimated using the ISO 6336 methodology [30,31].

2.2. Life estimation

It is well-known that contact and bending stress levels have a substantial effect on gear fatigue life. Fatigue failure takes place when these stresses exceed the permissible stresses. Estimation of these stresses involves consideration of fatigue resistance factors which account for the various influences on the life of the gears [32,33]. The calculated service life is based on the notion that every load cycle contributes to the damage of the gears. The amount of damage depends on the stress level, with levels below a defined value considered as non-contributory.

Fatigue resistance factors are required for life estimation; these factors are calculated using the ISO standard based on gear geometric and material specifications. A numerical tool was used to extract these features based on Method C of ISO 6336. The factors are summarized in Table 2, the details and physical meaning of these factors can be found in Refs. [32,33].

In order to estimate the gear life, bending and pitting stress spectra are required and this is calculated based on equation (2) [33].

Table 2
Fatigue resistance factors calculated based on ISO guidelines.

Parameter	Sun gear	Planet gears
Dynamic load K_V	1.001	
Transverse load factor (contact stress) $K_{H\beta}$	1.063	
Face load factor (root stress) $K_{F\beta}$	1.049	
Face load factor (contact stress) $K_{H\alpha}$ / $K_{F\alpha}$	1	
Zone factor Z_H	2.495	
Single pair tooth contact factors $Z_{B/D}$	1.03	1
Elasticity factor Z_E	189.812	
Contact ratio factor Z_ϵ	0.878	
Helix angle factor (contact) Z_β	1	
Life factor (contact) Z_{NT}	0.95	0.972
Lubricant factor (contact) Z_L	1.047	
Velocity factor Z_V	0.942	
Roughness factor Z_R	0.99	
Work hardening factor Z_W	1	
Size factor Z_X	1	
Tooth form factor Y_F	1.39	1.290
Stress correction factor Y_S	1.92	2.045
Stress correction factor Y_{ST}	2	
Helix angle factor (tooth root) Y_β	1	
Rim thickness factor Y_B	1	1
Deep tooth factor Y_{DT}	1	
Life factor (tooth root) Y_{NT}	0.91	0.928
Test relative notch sensitivity factor $Y_{\delta relT}$	0.99	0.996
Relative surface factor Y_{RrelT}	1.04	1.047
Size factor (tooth root) Y_X	0.97	0.97
Mean stress influences factor Y_M	1	1
Safety factors in pitting	1.25	1.313
Safety factors in tooth bending	2.56	2.652

$$\sigma_{fi} = 2000 \frac{T_i}{d_{ref} m_n b} Y_s Y_F Y_\beta K_{vi} K_{Bi} K_{\alpha i} \tag{2}$$

where T_i is the torque experienced by gear, σ_{fi} is nominal tooth root stress which is the maximum local principal stress produced at the tooth root when an error-free gear pair is loaded by the static nominal torque and without any pre-stress such as shrink fitting [33].

The contact stress spectrum is estimated by Ref. [32]:

$$\sigma_{Hi} = Z_H Z_E Z_\in Z_{BD} \sqrt{2000 \frac{T_i}{d_{ref}^2 b} \frac{u+1}{u} K_{vi} K_{H\beta} K_{H\alpha i}} \tag{3}$$

where σ_{Hi} is the contact stress at pitch point which is the stress due to the static nominal torque of error-free gears.

To account for variation of load distribution for the planetary gears the nominal stress spectrum for bending and contact are corrected [30,32,33], see equations (4) and (5).

$$\sigma_H = Z_B \sigma_{Hi} \sqrt{K_A K_V K_{H\beta} K_{H\alpha}} \tag{4}$$

$$\sigma_F = \sigma_{Fi}\ K_A K_V K_{F\beta} K_{F\alpha} \tag{5}$$

All factors used in the above equations are defined in Table 2. These stress spectra are used to estimate the life factors for pitting Z_{nt} and bending Y_{nt}.

$$Z_{nt} = \frac{\sigma_H}{\sigma_{HP}} \tag{6}$$

$$Y_{nt} = \frac{\sigma_{fi}}{\sigma_{fP}} \tag{7}$$

In turn, the life factor is used to estimate the corresponding number of cycles to failure for each load bin using the graphical

information in ISO 6336-2:2006, Fig. 6, and ISO 6336-3:2006, Fig. 9 Then, the damage index due to fatigue is calculated for each cycle using the Miner's rule [34].

$$D = \sum_{i=0}^{n} \frac{N_t}{N_i} \tag{8}$$

In which N_t is the number of cycles for one gear tooth and N_i is the total number of cycles in order to cause damage under corresponding loading conditions. This is estimated based on material fatigue characteristics described by the Wohler curve, as derived from material testing under cyclic loading. The test results are presented as a plot of stress (S) against the number of cycles to failure (N), known as an S-N curve; the international standard provides this data for gears material for both contact and bending stresses (ISO 6336-2:2006, and ISO 6336-3:2006) [32,33].

Remaining life prediction of gears are not only dependent on the load history experienced by the turbine, but also the expected future load. As the tidal cycle can be accurately predicted for specified locations using hydrodynamic ocean modelling system, see Ref. [40], therefore the average damage index per the tidal cycles D_a can be estimated using a load history. For purpose of this study the average damage index is calculated based on one tidal cycle due to lack of longer hydrodynamic data, however using longer hydrodynamic data could lead to more accurate average damage index per tidal cycle. The remaining life (L) is predicted by:

$$L = \frac{1 - D}{D_a} \tag{9}$$

The process of predicting the life described above is a continuous process and suitable for online gearbox prognostics as summarised in Fig. 4.

3. Hydrodynamic modelling

3.1. Blade element momentum theory (BEMT)

The synthetic torque records used in this paper were generated using a blade element momentum theory (BEMT) model of a tidal turbine. BEMT is a widely-employed technique [41–43] for modelling conventional horizontal-axis turbines, in both wind and tidal application. There is an extensive and well-rooted literature on the method [44] so a brief overview is presented here.

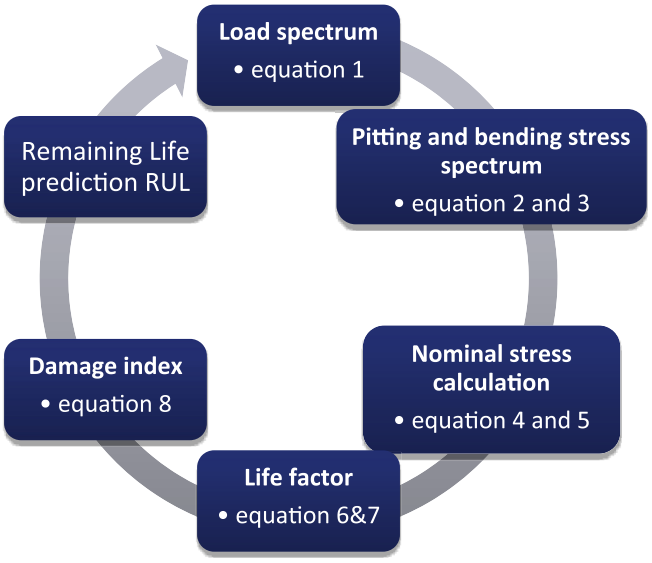

Fig. 4. The proposedprognostic process.

In essence, BEMT parameterises two different models of a turbine with parameters called 'induction factors', and then determines the value of the induction factors that brings these models into agreement. In the first place, the turbine was represented as a collection of annular rings, each of which absorbs some linear momentum from the flow of the fluid and imparts a degree of swirl into the wake. In the second place, the turbine was regarded as a collection of two-dimensional foils generating lift and drag forces that vary depending on the flow angle and velocity at the foil location. The annuli in the first representation and the blade elements in the second lie at the same radial locations, giving a one-to-one correspondence. The lift and drag coefficients are calculated from a lookup table that is chosen based on the specific foil used in the turbine design, and the forces themselves also depend on the chord length and angle of blade twist at each radial location.

The two induction factors (axial and tangential) indicate how much the momentum flux of the working fluid through each annular element is changed by the presence of the blades; they also affect the velocity of the fluid relative to each blade element and thus determine the hydrodynamic forces. Since the change of momentum flux and the hydrodynamic forces must be equivalent, the problem is reduced to finding the values of the induction factors that satisfy this requirement. There are a number of approaches to solving this problem; the method employed [43] treats it as a minimisation problem.

The BEMT is most commonly used to predict turbine performance in terms of power output. However, as the forces on each of the blade elements were calculated at each time step of the simulation the time-varying loads on the rotor can be calculated throughout the duration of the simulation by summing the tangential forces across all blades. This method has been employed to generate the torque records used in the current study. Although classical BEMT only allows steady uniform inflow, the model employed has been modified such that it can simulate a turbine subject to non-uniform, time-varying flows.

3.2. Synthetic eddy method (SEM)

Classical BEMT requires a steady, uniform inflow. In this new modified model, the ability to track the location of each two-dimensional foil has been added on each blade separately, allowing the simulation of unsteady and non-uniform flows. This capability allows out the work described in this paper to be carried.

This capability, of course, is of limited use if appropriate inflow data is not available. Ideally, measured field data should be used from a turbine deployment site; however, there is no device capable of taking simultaneous, high-frequency measurements of all three components of flow velocity across a volume of water large enough to contain a full-scale turbine. Instead, the synthetic eddy method (SEM) was employed to generate an artificial flow field that can be specified to arbitrary precision in both space and time.

The SEM was developed as a way of generating inflow data for Large Eddy Numerical simulations [45]. Again, an extensive description of SEM is beyond the scope of the current work, so a brief description only is provided here. Given a set of covariances for the fluctuation velocities of a turbulent flow field, along with a distribution of eddy length scales, SEM generates a time-varying field of eddies each of which induce velocities in a region of space near them. The input data requirements are easily met, as the most common method of gathering data on turbulence at planned deployment sites is with acoustic Doppler current profilers [46–48], and these measurement devices output precisely the type of statistical data that SEM requires as an input.

The synthetic eddies are characterised by a strength, which determines the magnitude of the induced velocities; a length scale, which determines the size of the region in which the eddies influence is present; and a shape function. With strengths derived from the input covariances and a suitably-normed shape function (see Ref. [45] for details), the second-order statistical moments of the artificial flow field will match those specified by the covariances used to calculate the eddy strengths. Note that this matching is only exact for a simulated flow-field of infinite duration.

4. Generation of the torque record

The geometry of a model turbine that has been extensively tested was employed in this study [49]. The model itself is too small to be effectively used in turbulent flows based on field data, as it would be significantly smaller than the smallest measured eddy length scales; therefore the authors elected to scale up the radius and chord length by a factor of 10, giving an overall rotor diameter of 4.75 m. The geometry characteristics of the blades of this turbine are shown in Fig. 5; a Wortmann FX 63-137 blade section is used for the entire blade span.

The Synthetic eddy method (SEM) was used to generate the inflow conditions based on measured field data. This field data used was taken from ADCP measurements in Ramsey Sound, a channel off the coast of Pembrokeshire, between the 13th and 27th of September, 2009; this encompasses a complete spring-neap cycle. Seven flood and ebb phases (i.e., fourteen phases in total) corresponding to regular intervals from the measurement period were selected as the test conditions for the work presented here. For each of these phases, the covariances needed to generate a synthetic turbulent field with SEM were calculated from an hour-long subset of ADCP data corresponding to the time of maximum current speed.

A full, three-dimensional velocity field of 10 min duration was generated from each of the fourteen sets of turbulence statistics. Fig. 6 shows an example of how the 'template' statistics taken from ADCP measurements are replicated in the synthetic turbulence field, the top three panels show autocovariance for each of the three velocity fluctuation components (u',v' and w') and the bottom two

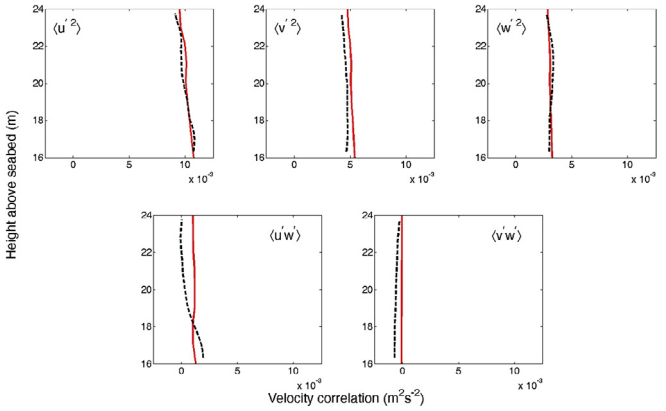

Fig. 6. Comparison of ADCP-measured turbulence statistics (solid red line) and statistics of synthetic turbulence created using SEM (dashed black line) for a representative tidal phase.

panels show horizontal-vertical cross-covariance (u'w' and v'w'), note that ADCPs cannot measure the horizontal-horizontal cross-covariance ⟨u'v'⟩; this is set to zero in the SEM model. The data for this example were taken from the first ebb phase of the spring-neap cycle considered. Complete knowledge of the flow velocities at any point was provided by the synthetic flow field. Therefore the covariances were calculated directly, by taking the time-average of the velocity fluctuation products over the duration of the synthetic flow field. The results show that the measured velocity covariances are well replicated by the SEM. By running one BEMT simulation for each of the velocity fields generated in this way, torque records were obtained and then used as inputs for the gearbox prognostic model.

5. Data processing

The numerically simulated data was classified into ebb and flood groups based on flow direction; flood corresponding to the tide

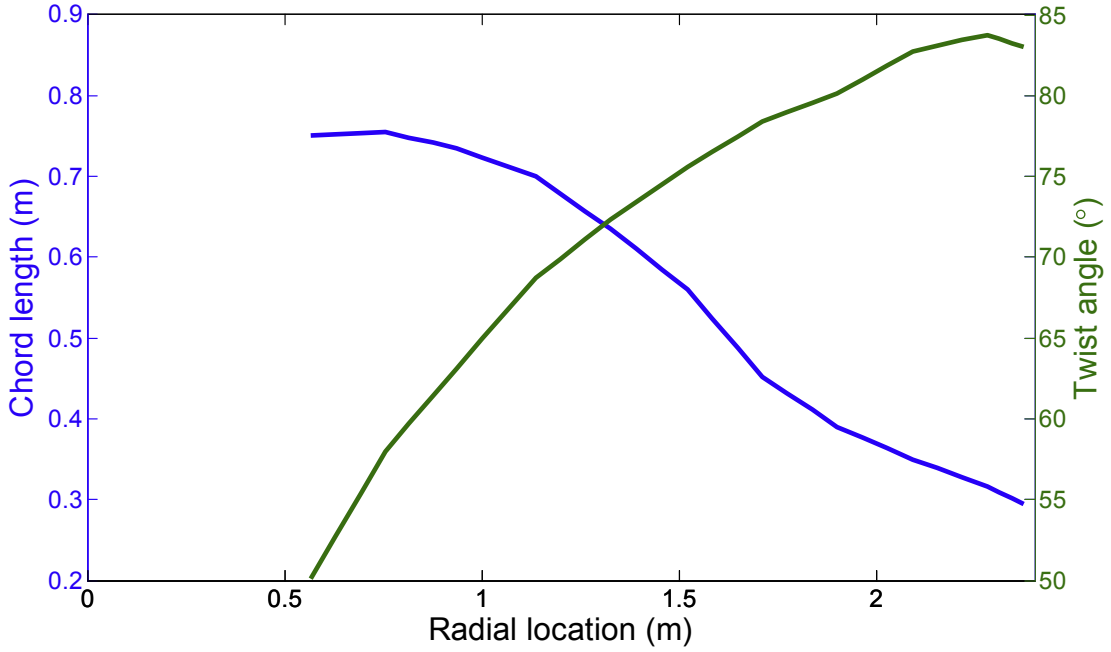

Fig. 5. Geometry characteristics of turbine blades used in the BEMT model.

flow into shore while ebb refers to the tide draining away from shore. Each flow was assumed to represent 50% of the lifetime and each flow contained 7 load classes, each class being represented by 10 min speed and torque data. The flow data used represents no-wave conditions.

The measured tide speed [24] was employed in the numerical simulation for generating turbine speed and torque data for one tidal cycle (14 days). This provided the load experienced by the transmission gearbox. A probability density function of the load was estimated by considering the cycle during each of the seven load classes which was then accumulated. This procedure was applied for both load and speed data as shown in Figs. 6 and 7. The load and speed probability distribution was used as the basis for predicting the load experienced by the gearbox throughout its life (see Fig. 8).

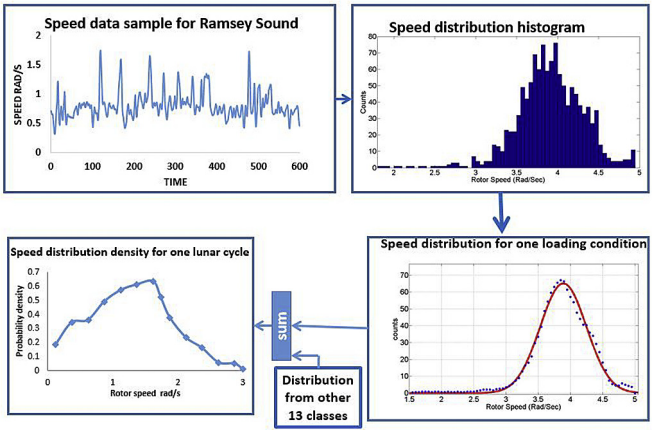

Fig. 8. Speed data processing.

6. Model output

The torque data from the numerical simulation was used to estimate the useful life based on the procedure described above. The calculations began by estimating the load spectra on the gears from the simulated torque and speed data. For the purposes of this illustration it was assumed the gearbox was 100% efficient. The stress spectra for both contact and bending were then determined from the load spectra, see Fig. 9.

The stress spectra, geometric features, fatigue resistance factors and the equations described previously were employed for estimating the damage index. For demonstration purpose the result of first stage sun gear is summarised in Fig. 9 and Table 3.

The analysis of the result shows that the sun gear of the first stage has a higher damage index for contact load (0.0032) compared to the bending load damage index (0.0026). In addition the contact stress was higher than the bending stress (Fig. 9) suggesting the gears are expected to fail due to pitting as opposed to a tooth bending failure; the expected life of first stage sun gear under these loading conditions is 157 lunar cycle which corresponds to approximately 13 years.

Load cycle data reduction has an impact on the accumulated damage index, therefore a sensitivity analysis on the effect of bin size when estimating the damage index was performed; the analysis was applied on the first stage sun gear and employed for one of load classes. The damage index was calculated using the different bin sizes of load spectrum. Following analysis it was noted that the use of a low number of bins results in overestimating of life, and at higher number of bins the damage index converges towards a constant damage index value, see Fig. 10. However the difference between lower and higher values of bin size is not significant (less than 1.2%), see Fig. 11. This implies that the choice of bin size has a minor effect on life prediction.

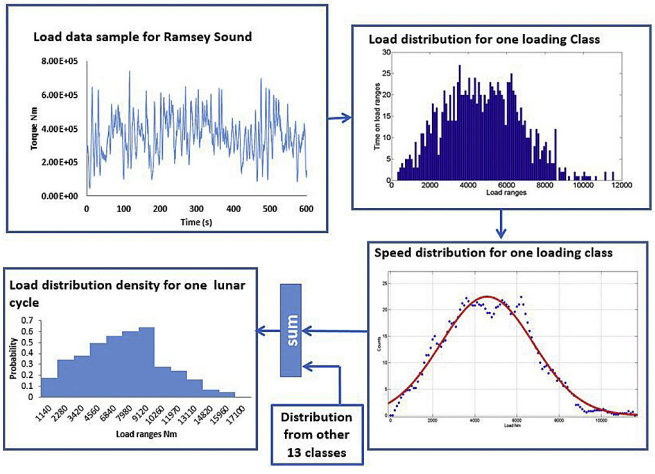

Fig. 7. Load data processing.

The analysis described thus far, as applied to the sun gear, was then employed to all gears in the different stages within the gearbox. The results are summarised in Table 4, and shows that the 3rd parallel stage has the shortest life whilst the highest damage index was noted on gears with the highest speed and smallest gear geometry. In addition results showed that the ring gears have a longer life due to the larger gear size. The result shows variations in the life and damage index of the gears which originate from geometrical variability and differences in stress cycles due to the differing rotational speeds.

7. Experimental demonstration

It was thought prudent to perform some validation of the proposed prognostic model. The validation was based on tests performed by Khan et al. [50] in which two pitting tests were performed on two identical pairs of case-hardened low carbon steel gears. The gears were tested under two loading conditions and the useful life was estimated based on ISO 6336-2 guidelines as described previously. The details of the gears used and the load conditions are summarized in Table 5.

The gear geometry and load conditions presented [48] were applied to the prognostic model developed by the authors and results showed pitting when the number of cycles reached 5.4×10^5 cycles during the first load condition and 1.08×10^6 cycles for the second load condition. Applying the Miner's sum using equation (3), the damage level was estimated at 0.92 for test 1 and 1.034 for test 2, (see Table 6). Visible pitting after gear testing is shown in Figs. 12 and 13. Observations from Figs. 12 and 13 show the presence of small pits at a time when the corresponding value of the Miner's sum (damage index) was approximately 1. This observation offered validation of the proposed prognostic methodology albeit at fixed load conditions.

8. Discussion

It has been shown that unsteady BEMT, in conjunction with SEM, can be used to predict some turbulence effects on TSTs, and to investigate how these effects can be ameliorated. The synthetic eddy method has been shown in Figs. 4 and 5 to yield a velocity field that, while non-physical, statistically reproduces measured

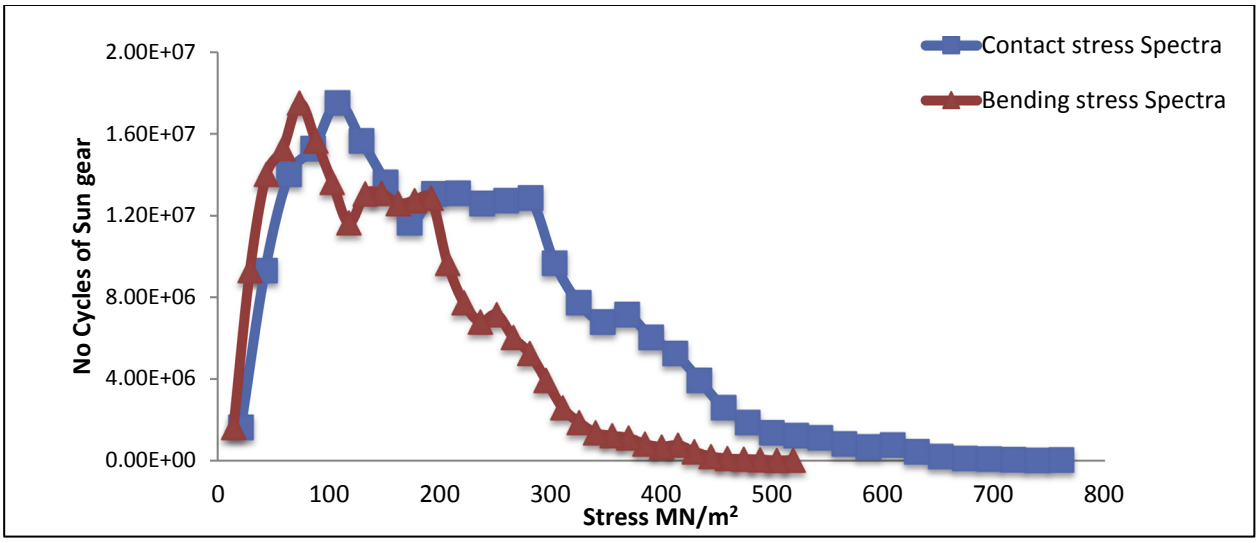

Fig. 9. Sun gear stress spectrum over one tidal cycle.

Table 3
First stage sun gear life.

Sun Gear pitting life	157.8 lunar cycles
Sun Gear Bending life	194.82 lunar cycles
Sun Gear pitting Damage index for over one lunar cycle	0.0032
Sun Gear Bending Damage index consumption over one lunar cycle	0.0026

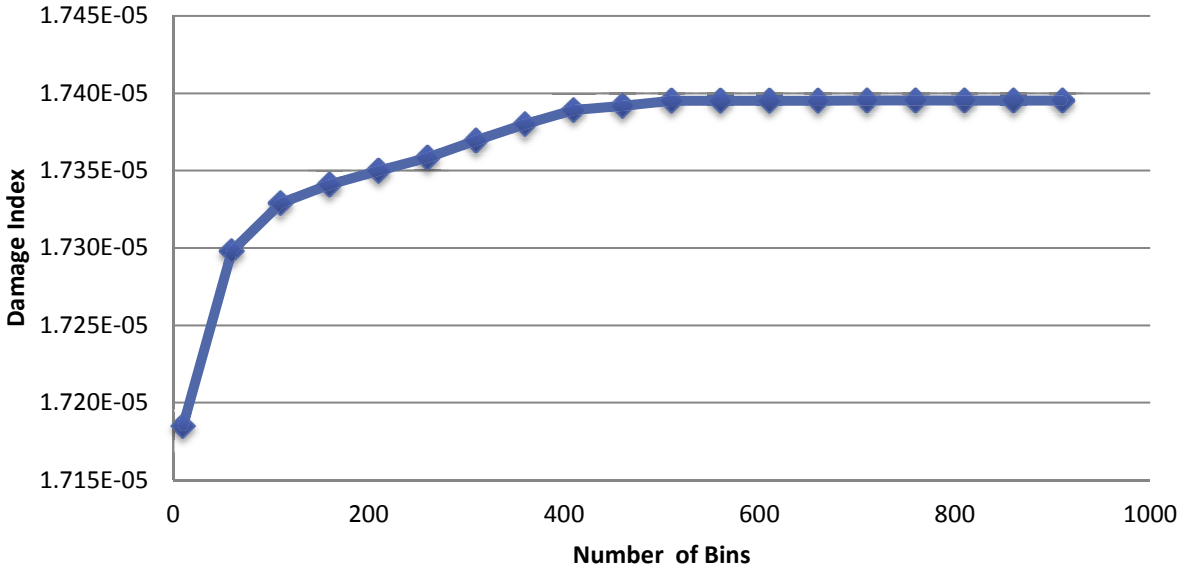

Fig. 10. Damage index convergence.

turbulence. This means this research was able to simulate a Tidal Stream Turbine's TST response to turbulence of known statistical properties without the need for either detailed velocity measurements or expensive computation.

The synthetic eddy method, although it provides satisfactory turbulent flowfields in a statistical sense, is not the only way of predicting fluctuating velocities on a TST. There are well-validated spectral methods that are widely used in the wind turbine industry, and some recent work has indicated that the spectral properties of tidal currents are sufficiently similar that these atmospheric methods could be adapted for use in marine flows [51]. A fruitful avenue of research, then, would be to attempt analysis of the test cases presented in this paper in the case where artificial turbulence is generated with spectral methods adapted for tidal flow, rather than with SEM.

The prognostics model developed focuses only on fatigue damage due to the contact and bending stresses. However, it should be noted that the effect of data sampling frequency in this analysis can lead to life overestimation due to the low sampling rate of synthetic data employed, especially for the high speed

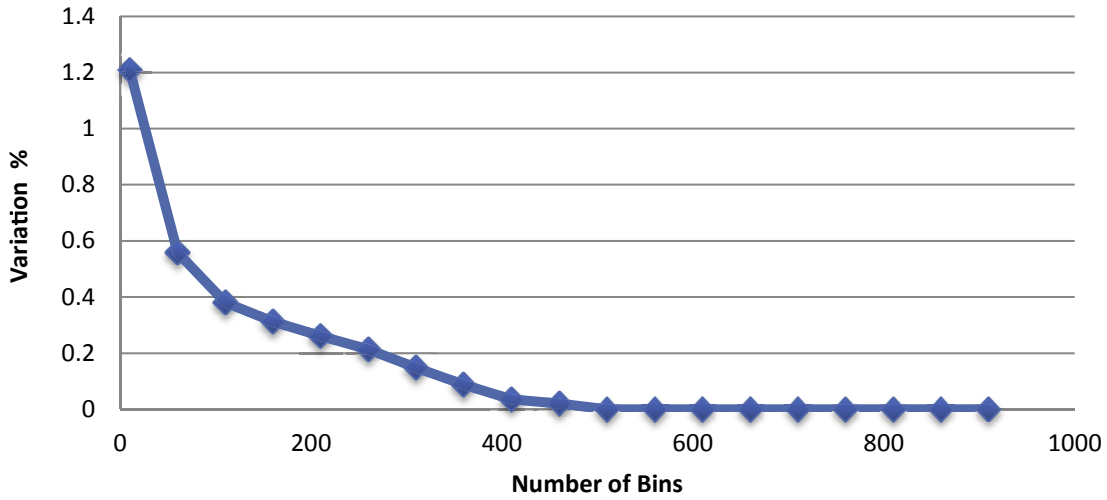

Fig. 11. Variation of result under different numbers of bins.

Table 4
Result of life prediction for gearbox component.

Components	Pitting life (No of lunar cycles)	Bending life (No of lunar cycles)	Pitting Damage index for over one lunar cycles	Bending Damage index for over one lunar cycles
Planets gear (1st stage)	232.05	335.82	0.0023	0.0014
Sun gear (1st stage)	157.8	194.8	0.0033	0.00257
Ring Gear (1st stage)	347.16	487.05	0.0015	0.0010
Planets gear (2nd stage)	238.25	356.8	0.0021	0.0001
Sun gear (2nd stage)	162.01	207.0	0.00311	0.0024
Ring Gear (2nd stage)	356.91	518.3	0.0014	0.0009
Pinion gear HSS	135.0	177.0	0.0038	0.0028
Wheel gear HSS	145.8	180.9	0.0035	0.0028

Table 5
Gear parameter according to design calculation (ISO6336.2) [50].

Gear	Specification
Helix angle	17.75 deg
Centre to distance	113.0 mm
No. of teeth	35.0
Reference diameter	110.2 mm
Load condition 1	6500 N
Load condition 2	4347 N
Speed	1000 RPM
Life estimated in load condition 1	5.985×10^5 cycles
Life estimated in load condition 2	9.67×10^5 cycles

Table 6
Model demonstration result.

	Test No. 1	Test No. 2
Actual Number of Cycles (from the test)	5.9×10^5	9.67×10^5
Predicted Number of Cycles	5.4×10^5	1.08×10^6
Predicted Damage Index	0.92	1.034

stage where a higher sampling frequency is required. The ISO standard for cycle counting states that [52], "The sampling frequency shall be such that every analog loading cycle is represented by at least 20 digital points at least 20 times that of the observed maximum frequency of the real or expected analog signal". The sampling frequency for the data employed was 20 Hz, which satisfied the requirement for analysis of the low speed gearbox stage. However for the high speed gear stages a sampling frequency 20 times the rotational frequency (24 Hz) is required, and therefore the life expectancy of the high speed stage should be calculated with a higher sampled torque data which was not available for this investigation. Even with the known life overestimation, the high speed stage (HSS) life was shorter than the other stages, and therefore damage is expected to initiate firstly in the gears of the high speed stage. This finding supports the observations of wind turbines failure, in which HSS failure were the most [53]. This is beneficial in not only giving an estimate for when maintenance ought to be scheduled, but also in identification of which components need to be redesigned or improved to lengthen the gearbox's fatigue life. It is worth considering that eleven years may be too pessimistic an estimate for the gear's lifespan, due to the fact that the probability distributions of load and speed that have been used are based on data from the fastest segments of flood and ebb phases across the spring-neap cycle, and thus they neglect both slack water and the less-intense portions of floods and ebbs. A probability distribution of loads that did incorporate these times with lower loading would almost certainly yield a longer fatigue life.

The gear life prediction results showed that the transmission system exposed to tidal currents will experience a shorter life compared to that exposed to wind load conditions. The gearbox considered in this study was designed to operate for 20 years (1.5–2 MW) however this analysis showed a 13 year life expectancy if this gearbox was employed in a tidal turbine, reiterating the influence on gear life for the very different loading conditions. The

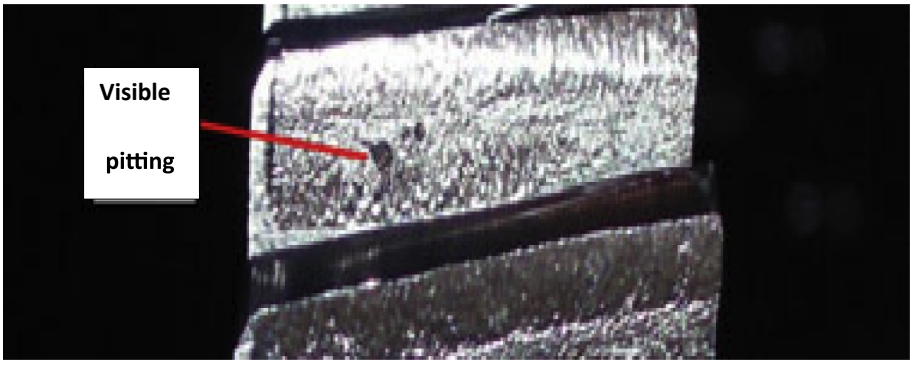

Fig. 12. Visible pitting after test 1 [50].

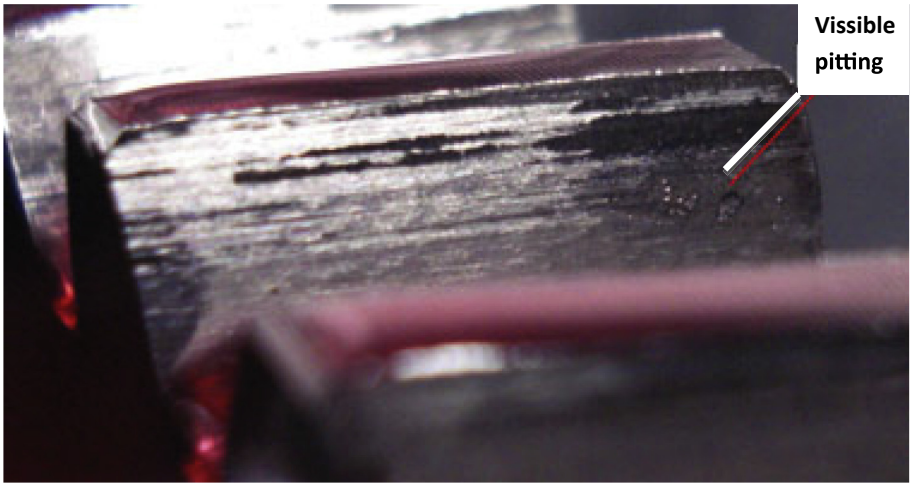

Fig. 13. Visible damage after test 2 [50].

prognostic concept was validated using constant load experimental data, however further experimental work is recommended to assess the prognostic model under variable load conditions.

9. Conclusion

A prognostic model based on the loading condition has been developed to predict the residual life of a gearbox during turbine operation. The model employed synthetic turbulence data generated for The Ramsey Sound region [25]. The prediction model encompass an element of a physic based (fracture mechanics) and data driven approach. The result shows life variations between the gears. These variations come from geometrical variability and differences in stress cycles due to the differing rotational speeds.

Furthermore it was noted that the high speed pinion has the highest damage index. This is mainly due to its higher number of cycles and lower number of teeth compared to the other gears. In addition the progression of surface pitting damage is expected prior to any damage at the gear root.

This study emphasizes that the life prediction depends on probability of loading condition, therefore a statistical significant data set will enhance prediction. In addition continuous updates of load cycle during the turbine operation will contribute to life prediction accuracy. The model was validated using constant load pitting test data and an accurate prediction of life was proved. However further experimental investigation is recommended to verify the effect of variable load and speed.

Acknowledgments

The authors would like to thank the SuperGen UK Centre for Marine Energy Research (UKCMER) for funding this research (EPSRC Grant EP/J010200/1). The authors acknowledge the financial support of the Welsh Assembly Government and Higher Education Funding Council for Wales through the Sêr Cymru National Research Network for Low Carbon, Energy and Environment.

References

[1] Digest of UK energy Statistics 2012, 12/089, Department of Energy and Climate Change, 2012. UK).
[2] Department of Trade and Industry, Economic Viability of a Simple Tidal Stream Energy CAPTURE DEVICE, 2007. TP/3/ERG/6/1/15527/REP, 2007, UK.
[3] S.E. Ben Elghali, M.E.H. Benbouzid, J.F. Charpentier, Marine tidal current electric power generation technology: state of the art and current status, in: Electric Machines & Drives Conference, 2007. IEMDC '07, vol. 2, IEEE International, 2007, p. 1407.
[4] J. Houde, Cost-benefit Analysis of Tidal Energy Generation in Nova Scotia: a Scenario for Tidal Farm with 300 MW of Installed Capacity in the Minas Passage in 2020 (Master Thesis), Dalhouseie University, Canada, 2012.
[5] P.J. Tavner, J. Xiang, F. Spinato, Reliability analysis for wind turbines, Wind Energy 10 (1) (2007) 1–18.
[6] A.I. Winter, Differences in fundamental design drivers for wind and tidal turbines, OCEANS, 2011 IEEE (2011) 1, 6-9 June 2011, Santander, Spain, uk.
[7] B. Rao, Handbook of Condition Monitoring, Elsevier, Oxford, UK, 1996, ISBN 185617 234 1.
[8] F. Spinato, P.J. Tavner, G.J.W. van Bussel, E. Koutoulakos, Reliability of wind turbine subassemblies, Renew. Power Gener. IET 3 (4) (2009) 387–401.
[9] R. Dupuis, Application of oil debris monitoring for wind turbine gearbox prognostics and health management, in: Annual Conference of the Prognostics

and Health Management Society, 2010, p. 10, 10-16 October, Portland.
[10] C. Crabtree, James, Condition Monitoring Techniques for Wind Turbines (Doctoral Thesis Thesis), Durham University, UK, 2011.
[11] Z. Hameed, Y.S. Hong, Y.M. Cho, S.H. Ahn, C.K. Song, Condition monitoring and fault detection of wind turbines and related algorithms: a review, Renew. Sustain. Energy Rev. 13 (1) (2009) 1–39.
[12] Wenxian Yang, P.J. Tavner, C.J. Crabtree, M. Wilkinson, Cost-effective condition monitoring for wind turbines, Ind. Electron. IEEE Trans. 57 (1) (2010) 263–271.
[13] D. Kitaljevich, R. Dupuis, M. Lu, Oil Debris Condition Monitoring for Wind Turbine Gearboxes, 2009. Beijing Wind Power, 21–23 October, Beijing, China.
[14] A. Sait, Y. Sharaf-Eldeen, A review of gearbox condition monitoring based on vibration analysis techniques diagnostics and prognostics, in: T. Proulx (Ed.), Rotating Machinery, Structural Health Monitoring, Shock and Vibration, vol. 5, Springer, New York, 2011, ISBN 978-1-4419-9427-1, pp. 307–324.
[15] P.W. Tse, D.P. Atherton, Prediction of machine deterioration using vibration based fault trends and recurrent neural networks, J. Vib. Acoust. Trans. ASME 121 (3) (1999) 355–362.
[16] V. Venkatasubramanian, R. Vaidyanathan, Y. Yamamoto, Process fault detection and diagnosis using neural networks—I. steady-state processes, Comput. Chem. Eng. 14 (7) (1990) 699–712.
[17] Xiaoli Li, Shiu Kit Tso, Jun Wang, Real-time tool condition monitoring using wavelet transforms and fuzzy techniques, Syst. Man, Cybern. Part C Appl. Rev. IEEE Trans. 30 (3) (2000) 352–357.
[18] B. Chen, P.J. Tavner, Y. Feng, W.W. Song, Y. Qiu, Bayesian Network for Wind Turbine Fault diagnosis.", Proceedings of European Wind Energy Association, European Wind Energy Association, Copenhagen, Denmark, 2012, 16–19 April.
[19] F. Elasha, D. Mba, C. Ruiz-Carcel, A comparative study of adaptive filters in detecting a naturally degraded bearing within a gearbox, Case Stud. Mech. Syst. Signal Process. 3 (2016) 1–8.
[20] F. Elasha, M. Greaves, D. Mba, in: F. Chaari, R. Zimroz, W. Bartelmus, et al. (Eds.), Diagnostics of a Defective Bearing within a Planetary Gearbox with Vibration and Acoustic Emission, Springer International Publishing, 2016, ISBN 978-3-319-20462-8, pp. 399–412.
[21] G.J. Kacprzynski, M.J. Roemer, A.J. Hess, Health management system design: development, simulation and cost/benefit optimization, in: Aerospace Conference Proceedings, 2002. IEEE, vol. 6, 2002, pp. 6–3065.
[22] S. Rudov-Clark, J. Stecki, C. Stecki, Application of advanced failure analysis results for reliability and availability estimations, in: Aerospace Conference, 2011 IEEE, 2011, p. 1.
[23] F. Elasha, D. Mba, J.A. Teixeira, Condition monitoring philosophy for tidal turbines, Int. J. Perform. Eng. 10 (5) (2014) 521.
[24] D. Paul, Why gearboxes fail and solution to lower derive train cost, available at: http://www.windpowerengineering.com/maintenance/why-gearboxes-fail-and-a-solution-to-lower-drivetrain-costs/, 2012. Accessed October/14.
[25] Tidal Energy Ltd, Tidal Energy Ltd, Cardiff, UK, 2009 (Ramsay Sound Current data UK).
[26] D. Mba, Prognostic opportunities offered by acoustic emission for monitoring bearings and gearboxes, in: Twelfth International Congress on Sound and Vibration, 2005.
[27] L.C.K. Reuben, D. Mba, Diagnostics and prognostics using switching Kalman filters, Struct. Health Monit. 13 (3) (2014) 296–306.
[28] K. Aslantaş, S. Taşgetiren, A study of spur gear pitting formation and life prediction, Wear 257 (11) (2004) 1167–1175.
[29] M. Pecht, R. Jaai, A prognostics and health management roadmap for information and electronics-rich systems, Microelectron. Reliab. 50 (3) (2010) 317–323.
[30] British Standards, Calculation of Load Capacity of Spur and Helical Gears - Part 1: Basic Principle, Introduction and General Infulunce Factors BS ISO 6336-1, BSI, UK, 2006.
[31] British Standards, Calculation of Load Capacity of Spur and Helical Gears - Part 6: Calculation of Service Life under Variable Load BS ISO 6336-6, BSI, UK, 2006.
[32] British Standards, Calculation of Load Capacity of Spur and Helical Gears - Part 2: Calculation of Tooth Contact Strength (BS ISO 6336-2), BSI, UK, 2006.
[33] British Standards, Calculation of Load Capacity of Spur and Helical Gears - Part 3: Calculation of Tooth Bending Strength (BS ISO 6336-3), UK, 2006.
[34] P., R, Dudley's Handbook of Practical Gear Design and Manufacture, second ed., CRC press, USA, 2012, ISBN 9781439866016.
[35] J.R. Cotrell, A preliminary evaluation of a multiple-generator drivetrain configuration for wind turbines, in: ASME 2002 Wind Energy Symposium, American Society of Mechanical Engineers, 2002, p. 345.
[36] K. Smolders, L. Long, Y. Feng, P.J. Tavner, Reliability analysis and prediction of wind turbine gearboxes, in: European Wind Energy Conference, 20–23 April 2010, 2010 (Warsaw, Poland, UK).
[37] A.W. Christopher, Wind Turbine Reliability: Understandingand Minimizing Wind Turbine Operationand Maintenance Costs, SAND2006–1100, Sandia National Laboratories, New Mexico, California, 2006.
[38] A. Ragheb, M. Ragheb, Wind turbine gearbox technologies, in: 1st International Nuclear & Renewable Energy Conference (INREC), 21-24 March, IEEE, Amman, 2010, p. 1.
[39] S. Sheng, P.S. Veers, Wind turbine drivetrain condition monitoring-an overview, in: Mechanical Failures Prevention Group: Applied Systems Health Management Conference, 10-12 May, National Renewable Energy Laboratory, Virginia, USA, 2011, p. 2.
[40] D.M. Culley, S.W. Funke, S.C. Kramer, M.D. Piggott, Integration of cost modelling within the micro-siting design optimisation of tidal turbine arrays, Renew. Energy 85 (2016) 215–227.
[41] W. Batten, A. Bahaj, A. Molland, J. Chaplin, Experimentally validated numerical method for the hydrodynamic design of horizontal axis tidal turbines, Ocean. Eng. 34 (7) (2007) 1013–1020.
[42] W.Z. Shen, R. Mikkelsen, J.N. Sørensen, C. Bak, Tip loss corrections for wind turbine computations, Wind Energy 8 (4) (2005) 457–475.
[43] I. Masters, J. Chapman, J. Orme, M. Willis, A robust blade element momentum theory model for tidal stream turbines including tip and hub loss corrections, Proc. IMarEST-Part A-J. Mar. Eng. Technol. 10 (1) (2011) 25–35.
[44] T. Burton, N. Jenkins, D. Sharpe, E. Bossanyi, Wind Energy Handbook, second ed., John Wiley & Sons, UK, 2011, ISBN 978-0-470-69975-1.
[45] N. Jarrin, S. Benhamadouche, D. Laurence, R. Prosser, A synthetic-eddy-method for generating inflow conditions for large-eddy simulations, Int. J. Heat Fluid Flow 27 (4) (2006) 585–593.
[46] J.H. Simpson, N.R. Fisher, P. Wiles, Reynolds stress and TKE production in an estuary with a tidal bore, Estuar. Coast. Shelf Sci. 60 (4) (2004) 619–627.
[47] Y. Lu, R.G. Lueck, Using a broadband ADCP in a tidal channel. Part II: Turbulence, J. Atmos. Ocean. Technol. 16 (11) (1999) 1568–1579.
[48] J. Thomson, B. Polagye, V. Durgesh, M.C. Richmond, Measurements of turbulence at two tidal energy sites in Puget Sound, WA, Ocean. Eng. IEEE J. 37 (3) (2012) 363–374.
[49] S. Tedds, I. Owen, R. Poole, Near-wake characteristics of a model horizontal axis tidal stream turbine, Renew. Energy 63 (2014) 222–235.
[50] M.A. Khan, D. Cooper, A. Starr, BS-ISO helical gear fatigue life estimation and wear quantitative feature analysis, Strain 45 (4) (2009) 358–363.
[51] I.A. Milne, R.N. Sharma, R.G. Flay, S. Bickerton, Characteristics of the turbulence in the flow at a tidal stream power site, Philos. Trans. Ser. A, Math. Phys. Eng. Sci. 371 (1985) (2013) 20120196.
[52] ISO standard, ISO 12110-2:2013 Metallic Materials – Fatigue Testing – Variable Amplitude Fatigue Testing – Part 2: Cycle Counting and Related Data Reduction Methods, the International Organization for Standardization, 2013.
[53] H. Link, W. Lacava, J. Van Dam, B. McNiff, S. Sheng, R. Wallen, M. MCdade, S. Lambert, S. Butterfield, F. Oyague, Gearbox Reliability Collaborative Project Report: Findig from Phase 1 and Phase 2 Testing, NREL/TP-5000–51885, National Renewable Energy Laboratory, USA, 2011.